DNA Adduct Formation by Platinum Anticancer Drugs. Insight into an Unusual GpG Intrastrand Cross-Link in a Hairpin-like DNA Oligonucleotide Using NMR and Distance Geometry Methods

Marian Iwamoto, Srinivasan Mukundan, Jr., and Luigi G. Marzilli*

Contribution from the Department of Chemistry, Emory University, Atlanta, Georgia 30322

*Received November 17, 1993**

Abstract: Treatment of a self-complementary duplex with Pt anticancer drugs leads to formation of an unusual type of hairpin-like oligonucleotide, Pt(A_2){5′d($A_1T_2G_3G_4$*G_5*$T_6A_7C_8C_9C_{10}A_{11}T_{12}$)3′} ($A_2$ = *cis*-$(NH_3)_2$ or ethylenediamine (en) and G*'s are platinated at N7). In previous NMR studies, several residues exhibited abnormal upfield- and downfield-shifted ^{1}H and ^{31}P signals, and one aromatic ^{1}H signal, G_4*H8, could not be located. In the present study, we found the G_4*H8 signal to be broad and shifted ~2 ppm upfield into the H1′ spectral region. This shift change is much larger than the theoretical maximum (<1 ppm) predicted for an unstrained structure, suggesting the platination site is strained. Distance geometry (DG) structures were calculated from NMR data in order to elucidate the structural basis for the unique properties of these species, including the unusual NMR shifts. At the platination site, the Pt(en) moiety is located in the major groove, and the platinum-bound G's both possess some unusual features; G_4* has an N sugar conformation and G_5* has a *syn* conformation. The *syn* G_5* base is oriented perpendicular to the Pt coordination plane. In contrast, the G_4* base is almost coplanar with this plane; the unusual orientation forces G_4*H8 into a close (≤3 Å) clash with the five-membered ring of G_5*. This proximity explains the substantial upfield shift observed for G_4*H8. The broadness of the G_4*H8 signal could be explained by minor vacillations about the Pt–N7(4) bond, which would sweep G_4*H8 across different shielding regions of the anisotropic G_5* base. The A_7 base in DG models is tucked inside the hairpin loop, with A_7H8 close to G_5*H8. A_7 is correctly oriented to explain (a) the G_4*H2′ shift into the methyl region of the ^{1}H spectrum, (b) the strong A_7H8 to G_5*H8 NOE, and (c) the downfield-shifted A_7H8 signal (caused by G_5* deshielding). The unprecedented downfield ^{31}P shift of A_7pC_8 is a result of an *anti,anti* conformation about the ζ,α torsion angles induced by a distortion in the backbone needed to allow G_4*C_9 Watson–Crick base pairing at the top of the stem. A B-DNA-like helical stem was found with base pairing between the first four bases of the 3′ and 5′ ends (A_1T_{12}, T_2A_{11}, G_3C_{10}, and G_4*C_9). These features are supported by 2D NOESY-in-H_2O data. Such hairpin-like structures, induced by the need to balance DNA and Pt structural demands, could form in palindromic regions of DNA and could be instrumental in platinum drug activity.

Introduction

An unusual hairpin-like dodecadeoxyribonucleotide,[1-3] Pt(A_2)-{5′d($A_1T_2G_3G_4$*G_5*$T_6A_7C_8C_9C_{10}A_{11}T_{12}$)3′} ($A_2$ = *cis*-$(NH_3)_2$ or ethylenediamine (en) and G*'s are platinated at N7), was discovered to form from the self-complementary duplex in studies directed at understanding the DNA interaction of *cis*-Pt(II)-$(NH_3)_2Cl_2$ and its analogues. These widely used anticancer drugs cross-link GpG sites in DNA.[4] The role of adduct formation is not fully understood, but structural perturbations in DNA may be a key factor. Regardless of their relevance to the anticancer activity of the Pt drugs, the unprecedented structural features in the adduct were suspected to be of intrinsic interest, from both a structural and a spectroscopic viewpoint. Unusual structures help to define spectroscopic and theoretical parameters, *e.g.* force fields in molecular mechanics calculations. Furthermore, an anticancer role for such hairpins is conceivable.

The previously studied platinated oligonucleotide (Pt(A_2)/12-mer) has two downfield-shifted ^{31}P signals, while most adducts have only one. Hairpin formation can explain the large size of the downfield ^{31}P signal in polymeric DNA caused by Pt anticancer drugs; the signal size could not be explained previously.[3] In addition, the formation of related hairpin-like structures in the palindromic sequence of DNA is believed to be important in gene control mechanisms;[5-13] hairpins have been found in gene transcription regions and origins of DNA replication. These anomalous structures could be involved in the critical positioning of regulatory proteins in phases of transcription and replication.[12,13] Proteins have been identified which recognize cisplatin-modified DNA.[14-17] For example, recently, a structure-specific recognition protein (SSRP1) and a homologous high-mobility group 1 protein

* Abstract published in *Advance ACS Abstracts*, June 1, 1994.

(1) Kline, T. P.; Marzilli, L. G.; Live, D.; Zon, G. *Biochem. Pharmacol.* **1990**, *40*, 97–113.
(2) Marzilli, L. G.; Mukundan, S., Jr.; Xu, Y.; Zon, G.; Bergman, A.; Yohannes, P.; Reily, M. D. In *Platinum and Other Metal Coordination Compounds in Cancer Chemotherapy*; Howell, S. B., Ed.; Plenum Press: New York, 1991; pp 101–14.
(3) Yohannes, P. G.; Zon, G.; Doetsch, P. W.; Marzilli, L. G. *J. Am. Chem. Soc.* **1993**, *115*, 5105–10.
(4) Sherman, S. E.; Lippard, S. J. *Chem. Rev.* **1987**, *87*, 1153–81.
(5) Blommers, M. J. J.; Walters, J. A. L. I.; Haasnoot, C. A. G.; Aelen, J. M. A.; van der Marel, G. A.; van Boom, J. H.; Hilbers, C. W. *Biochemistry* **1989**, *28*, 7491–8.
(6) Lilley, D. M. J.; Sullivan, K. M.; Murche, A. I. H. In *Nucleic Acids and Molecular Biology*; Eckstein, F., Lilley, D. M. J., Eds.; Springer-Verlag: New York, 1987; pp 126–37.
(7) Pramanik, P.; Kanhouwa, N.; Kan, L.-S. *Biochemistry* **1988**, *27*, 3024–31.
(8) Rajeswari, M. R.; Bose, H. S.; Kukreti, S.; Gupta, A.; Chauhan, V. S.; Roy, K. B. *Biochemistry* **1992**, *31*, 6237–41.
(9) Rentzeperis, D.; Kharakoz, D. P.; Marky, L. A. *Biochemistry* **1991**, *30*, 6276–83.
(10) Wolk, S. K.; Hardin, C. C.; Germann, M. W.; van de Sande, J. H.; Tinoco, I., Jr. *Biochemistry* **1988**, *27*, 6960–7.
(11) Xodo, L. E.; Manzini, G.; Quadrifoglio, F.; van der Marel, G. A.; van Boom, J. H. *Biochemistry* **1988**, *27*, 6321–6.
(12) Benight, A. S.; Wang, Y.; Amaratunga, M.; Chattopadhyaya, R.; Henderson, J.; Hanlon, S.; Ikuta, S. *Biochemistry* **1989**, *28*, 3323–32.
(13) Weaver, D. T.; DePamphilis, M. L. *J. Mol. Biol.* **1984**, *180*, 961–86.
(14) Chu, G.; Chang, E. *Science (Washington, D.C.)* **1988**, *242*, 564–7.
(15) Hughes, E. N.; Engelsberg, B. N.; Billings, P. C. *J. Biol. Chem.* **1992**, *267*, 13520–7.
(16) Pil, P. M.; Lippard, S. J. *Science (Washington, D.C.)* **1992**, *256*, 234–7.

0002-7863/94/1516-6238$04.50/0

(HMG1) were identified by Lippard and co-workers to be cisplatin-modified DNA-binding proteins.[16,17] These proteins could possibly recognize a variety of Pt–DNA lesions including hairpin-like structures and, thus, could be important for anticancer activity.

Unexpected biochemical behavior was demonstrated for the Pt(A_2)/12-mer in gel electrophoretic studies, which eventually established the G_4*pG_5* cross-link.[3] The adduct was not readily either 3′- or 5′-end-labeled, a behavior attributed to a suspected stability of base pairing in the stem. A particularly puzzling feature found in earlier extensive NMR studies of the Pt(en) derivative was the absence of the G_4*H8 signal from the aromatic region.[1,2] Other unusual spectroscopic features noted previously include (i) the A_7pC_8 ^{31}P signal is shifted downfield; (ii) a very strong G_5*H8-H1′ NOE is present, indicating a *syn* χ torsion angle; (iii) a strong A_7H8-G_5*H8 NOE is evident; (iv) the A_7H8 signal is shifted downfield; and (v) the G_4*H2′ signal is shifted into the methyl region.

To gain insight into the causes of these anomalies, we have carried out additional 2D homonuclear and heteronuclear NMR studies on Pt(en){d(ATGG*G*TACCCAT)-*N7(4),N7(5)*}. In this report, we briefly describe some new ^{13}C, ^{31}P, and ^{1}H assignments, including the missing H8 signal. We also describe in detail the use of the NMR data in distance geometry calculations to obtain three-dimensional models, which account for the unusual features of this hairpin-like species. The overall shape is unique.

Experimental Section

During the course of this investigation several samples were prepared and numerous 2D NMR studies (^{1}H–^{1}H NOESY, ^{1}H–^{1}H DQF-COSY, ^{1}H–^{13}C HMQC, ^{1}H–^{13}C HMBC, ^{1}H–^{31}P RCSC, and ^{1}H–^{1}H NOESY-in-H_2O) were performed. Details are available[18,19] and will be published elsewhere.

Distance Geometry. Distance geometry (DG) calculations were performed on a Silicon Graphics 4D/25 Personal Iris computer using DSPACE 4.0 (Hare Research, Inc., Bothell, WA).[20]

(a) Hydrogen Bonding, Torsion Angles, and Distance Information. Data regarding the presence of hydrogen bonds were acquired from 1D and 2D NMR spectral data taken in H_2O. Backbone torsion angles were determined mostly from the DQF-COSY spectrum as well as the RCSC spectrum using the Karplus relationship. Backbone torsion angles (α, β, γ, ϵ, ζ) were analyzed in a manner similar to the one previously described by Kim *et al.*[21] In a qualitative manner, a general range of coupling constants was assessed for several ^{1}H–^{1}H and ^{1}H–^{31}P pairs. The β (P–O–C5′–C4′) and ϵ (C4′–C3′–O–P) angles were determined from four-bond $J_{P-H4'}$ coupling and three-bond $J_{H3'-P}$ coupling, respectively.[22] The γ (O–C5′–C4′–C3′) torsion angles were evaluated from $J_{H5'/5''-H4'}$ coupling as well as NOE contacts. Sugar conformations, incorporating the δ (C5′–C4′–C3′–O) torsion angles, were assessed from carbon chemical shift data.[23,24] Torsion angles α (O–P–O–C5′) and ζ (C3′–O–P–O) were obtained from correlation with phosphorus chemical shifts.[25,26]

Initial distance information was obtained from NOESY buildup data[19] where NOE buildup and decay curves were obtained by plotting cross peak and auto peak volumes, respectively, against a range of mixing times. A two-spin approximation was used to estimate interproton separations.[27] The intensities of the dipole–dipole contacts were calibrated against a reference distance (cytosine H5–H6; 2.46 Å); a constant τ_c was assumed. All NOE contacts were then categorized into four broad groups according to cross peak intensity.[28] Each group was given a generous distance range: small, 2.0–5.5 Å; medium, 2.0–4.5 Å; large, 2.0–3.5 Å; and very large, 1.5–2.5 Å.

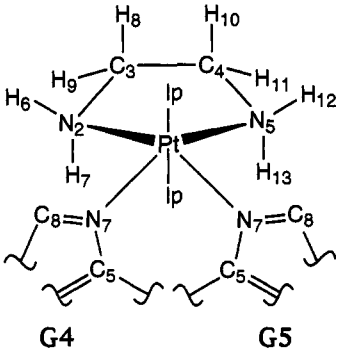

Figure 1. DSPACE template labeling scheme for the Pt(en) residue.

Torsion angles were incorporated into the DG calculations first by converting the angular data into distances. ζ and α angles were loosely constrained by O1P to C3′ and O2P to C5′, respectively. *Anti* interactions were defined as distance bounds between C3′ and O5′ (ζ) and between O3′ and C5′ (α). β *anti* angles were defined by P to O3′ distance constraints. γ torsion angles were defined by distance constraints between H4′ and H5′ and between H4′ and H5″. The sugar puckers, incorporating δ, were defined by several distance constraints. For S sugars, the following constraints were used: (i) C5′ to O3′, (ii) O3′ to H2′, and (iii) H2′ to H1′. For N sugars, the following were used: (i) H4′ to H3′, (ii) H3′ to H2″, and (iii) H3′ to N1/N9. Constraints for -*ac* ϵ torsion angles were defined by distance bounds between H3′ and P.

(b) Definition Files. The atom and pseudoatom definitions for H, C, N, O, P, and Me were from DSPACE. For Pt, two axial lone pairs were added to the Pt center, creating a pseudooctahedral structure. The lone pairs provided rigidity to the Pt square plane and allowed us to mimic the d_{z^2} orbital with the available version of DSPACE. Platinum was given a van der Waals radius of 1.38 Å with a dsp^2 hybridization.[29] Lone pair (lp) electrons were designed to have an overall distance of 1.3 Å from the center of the Pt to the edge of the electron cloud based on the van der Waals radius of the Pt.

The residue files in DSPACE were slightly modified, particularly those involving P, to agree with crystallographic data compiled by Saenger.[30] The Pt(en) residue file (Figure 1) and Pt(en) to G_4*pG_5* link file were constructed from crystallographic data on several Pt compounds.[31–33] The N7–Pt–N7 angle of 88.3° was obtained from *cis*-[Pt(NH_3)$_2$-{d(pGpG)}].[33] The N2–Pt–N5 angle of the Pt(en) moiety (84.3°) was defined according to [Pt(en)(7,9-dimethylhypoxanthine)$_2$](PF_6)$_2$.[32] The N7(4)–Pt–N2 (91.8°) and N7(5)–Pt–N5 (90.8°) angles were obtained from *cis*-[Pt(NH_3)$_2$(guanosine)$_2$]$^{2+}$.[31] The two coordinated guanosines in this structure are structurally distinct; one nucleoside was arbitarily chosen to represent G_4* and the other G_5*. The difference between the N2–Pt–N5 angles of the Pt-guanosine (89.3°) and the Pt-7,9-dimethylhypoxanthine (84.3°) structures had to be taken into account since a combination of angles was utilized in the square planar Pt template. The difference in the two N2–Pt–N5 angles was calculated (5.0°) and distributed equally between the Pt-guanosine ∠N7(4)–Pt–N2 and ∠N7(5)–Pt–N5, resulting in angles of 94.3° and 93.3° for ∠N7(4)–Pt–N2 and ∠N7(5)–Pt–N5, respectively. ∠C5–N7–Pt and ∠C8–N7–Pt for both G residues from the Pt-guanosine crystal structure[31] were modified to take into consideration the fixed C5–N7–C8 angle (103.8°) of the supplied guanine template. These modifications were necessary in order to keep

(17) Bruhn, S. L.; Pil, P. M.; Essigmann, J. M.; Housman, D. E.; Lippard, S. J. *Proc. Natl. Acad. Sci. U.S.A.* **1992**, *89*, 2307–11.
(18) Iwamoto, M. Ph.D. Dissertation Thesis, Emory University, 1993.
(19) Mukundan, S., Jr. Ph.D. Dissertation Thesis, Emory University, 1991.
(20) Banks, K. M.; Hare, D. R.; Reid, B. R. *Biochemistry* **1989**, *28*, 6996–7010.
(21) Kim, S.-G.; Lin, L.-J.; Reid, B. R. *Biochemistry* **1992**, *31*, 3564–74.
(22) Blommers, M. J. J.; van de Ven, F. J. M.; van der Marel, G. A.; van Boom, J. H.; Hilbers, C. W. *Eur. J. Biochem.* **1991**, *201*, 33–51.
(23) Mukundan, S., Jr.; Xu, Y.; Zon, G.; Marzilli, L. G. *J. Am. Chem. Soc.* **1991**, *113*, 3021–7.
(24) Santos, R. A.; Tang, P.; Harbison, G. S. *Biochemistry* **1989**, *28*, 9372–8.
(25) Powers, R.; Jones, C. R.; Gorenstein, D. G. *J. Biomol. Struct. Dyn.* **1990**, *8*, 253–94.
(26) Roongta, V. A.; Jones, C. R.; Gorenstein, D. G. *Biochemistry* **1990**, *29*, 5245–58.
(27) Noggle, J. H.; Schirmer, R. E. *The Nuclear Overhauser Effect*; Academic Press, Inc.: New York, 1971.
(28) Summers, M. F.; South, T. L.; Kim, B.; Hare, D. R. *Biochemistry* **1990**, *29*, 329–40.
(29) *Lange's Handbook of Chemistry*; 14th ed.; Dean, J. A., Ed.; McGraw-Hill, Inc.: New York, 1992.
(30) Saenger, W. *Principles of Nucleic Acid Structure*; Springer-Verlag, Inc.: New York, 1984.
(31) Cramer, R. E.; Dahlstrom, P. L.; Seu, M. J. T.; Norton, T.; Kashiwagi, M. *Inorg. Chem.* **1980**, *19*, 148–54.
(32) Kistenmacher, T. J.; de Castro, B.; Wilkowski, K.; Marzilli, L. G. *J. Inorg. Biochem.* **1982**, *16*, 33–46.
(33) Sherman, S. E.; Gibson, D.; Wang, A. H.-J.; Lippard, S. J. *J. Am. Chem. Soc.* **1988**, *110*, 7368–81.

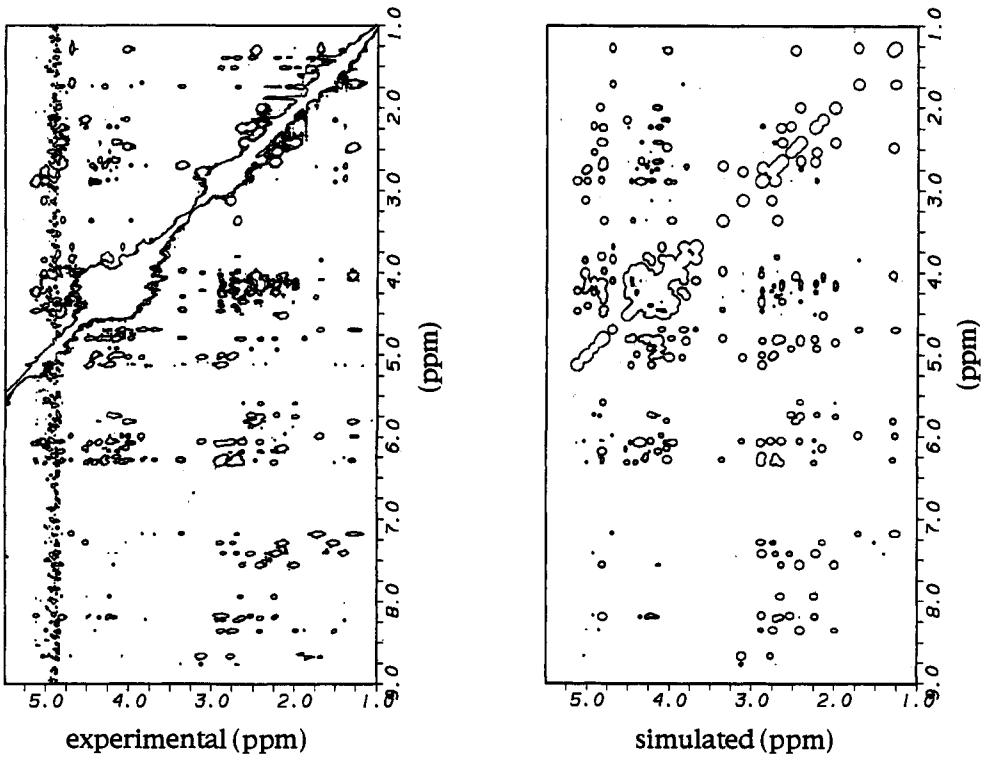

Figure 2. Back-calculated and experimental NOESY spectra of the Pt(en)/12-mer (500 ms).

the atoms Pt, N7, C8, and C5 planar. The guanine template C5–N7–C8 angle is slightly smaller than the Pt-guanosine C5–N7–C8 angles (104.9° (G_4*) and 104.3° (G_5*)); once again, a difference was taken between the angles. Half the difference in the C5–N7–C8 angles (1.1° (G_4*) and 0.5° (G_5*)) was added to both the Pt-guanosine C5–N7–Pt and C8–N7–Pt angles. The resulting angles follow: ∠C5(4)–N7(4)–Pt, 129.6°; ∠C8(4)–N7(4)–Pt, 126.3°; ∠C5(5)–N7(5)–Pt, 130.9°; and ∠C8(5)–N7(5)–Pt, 125.2°.

The C–C, C–N, and Pt–N bond lengths in the en moiety were taken from the Pt-7,9-dimethylhypoxanthine structure.[32] Idealized hydrogen atom positions in the en substructure were calculated with the MacroModel molecular modeling program.[34] H–C and H–N bond lengths as well as relevant bond angles were calculated from these positions.

(c) Bounds Matrix and Structure Generation. Experimental constraints (NOE contacts, hydrogen bonds, torsion angles, as well as other structural data) were placed in the bounds matrix, which was subsequently subjected to a smoothing algorithm. From this, trial starting structures were generated through the creation of a number of distance matrices and metric matrices.[35,36]

(d) Structure Refinement. The embedded structures were treated with several refining algorithms to optimize the structure coordinates to represent more accurately the defined constraints. The embedded structures were treated to multiple cycles of conjugate gradient refinement, simulated annealing, and generous coordinate randomization in order to thoroughly sample conformational space. Refined structures were correlated with experimental data assessing covalent and experimental deviations as well as nonbonded contact errors.[35] Penalty violations calculated by DSPACE were computed with all normalization weighting constants set to 1 with the exception of K_{linears}, which was set to 1.5. For each bounds matrix created, 300 refined structures were generated in each series. Over 3000 DG structures were created, and the low-penalty structures were analyzed.

(e) Back-Calculation. Simulated NOESY spectra were back-calculated from low-penalty structures in each series using the programs BKCALC and GNOESY (Hare Research, Inc., Bothell, WA).[20] Back-calculated spectra were graded according to visual deviations present between simulated and experimental spectra at mixing times of 100 and 500 ms (Figure 2). If major corrections were needed, the bounds file was altered and the refinement cycle was continued. This always led to an improvement of structures and subsequent improvement of simulated spectra. In addition, similarity of the low-penalty structures was also enhanced.

(f) Assessment of Low-Penalty Structures. After several cycles of refinement were conducted, the visual comparison between back-calculated and experimental spectra was terminated when no further improvements to the back-calculated spectrum could be made. At this point, the experimental and simulated buildup curves were normalized and visually compared (*e.g.* Figure 3).

The low-penalty structures (bottom 5%) in two series (selected because the structures in each represent the extremes of the location of the dynamic T_6 residue (*vide infra*)) are described in the supplementary material: (i) RMSDs calculated using all of the atoms including hydrogens; (ii) overlays of some structures, which have an average RMSD of less than 0.8 Å; (iii) RMSD penalty values; and (iv) total penalty violations ranked per residue and per atom (top 15%) and all bounds violations > 0.5 Å for one structure in each series.

Results and Discussion

NMR. In the original ^{1}H NMR assignment of the Pt(en)/12-mer,[1] the G_4* and G_5* residues were not assigned because the apparent absence of one aromatic signal precluded the normal sequential "walk". The signals were later assigned by using other connectivities, but the G_4*H8 signal was not found. We discovered the missing aromatic signal for G_4* from HMQC and from new NOESY data at 30 °C on a sample more concentrated than those used in the past. In this 30 °C NOESY spectrum, a weak cross peak was found in the base–base region; this cross peak correlates the G_5*H8 signal to a new aromatic signal that is much too weak to belong to the major species. The cross peak is undoubtedly not an NOE peak but rather an exchange peak between the hairpin-like form and a second, minor form, postulated to be a platinated duplex (*vide infra*). Exchange between these two forms is fast enough to give cross peaks in the 30 °C but not in the 5 °C NOESY spectrum. If G_5*H8 has an exchange partner, we reasoned that the G_4*H8 signal should have an exchange

(34) Still, W. C.; Mohamdi, F.; Richards, N. G. J.; Guida, W. C.; Lipton, M.; Liskamp, R.; Chang, G.; Hendrickson, T.; DeGunst, F.; Hasel, W. *MacroModel V. 2.5*; Department of Chemistry, Columbia University: New York, 1988.

(35) *DSPACE V. 4.0 Users Manual*; Hare Research, Inc.: Woodinville, WA, 1990.

(36) Crippen, G. M. *Distance Geometry and Conformational Calculations*; Research Studies Press: New York, 1981.

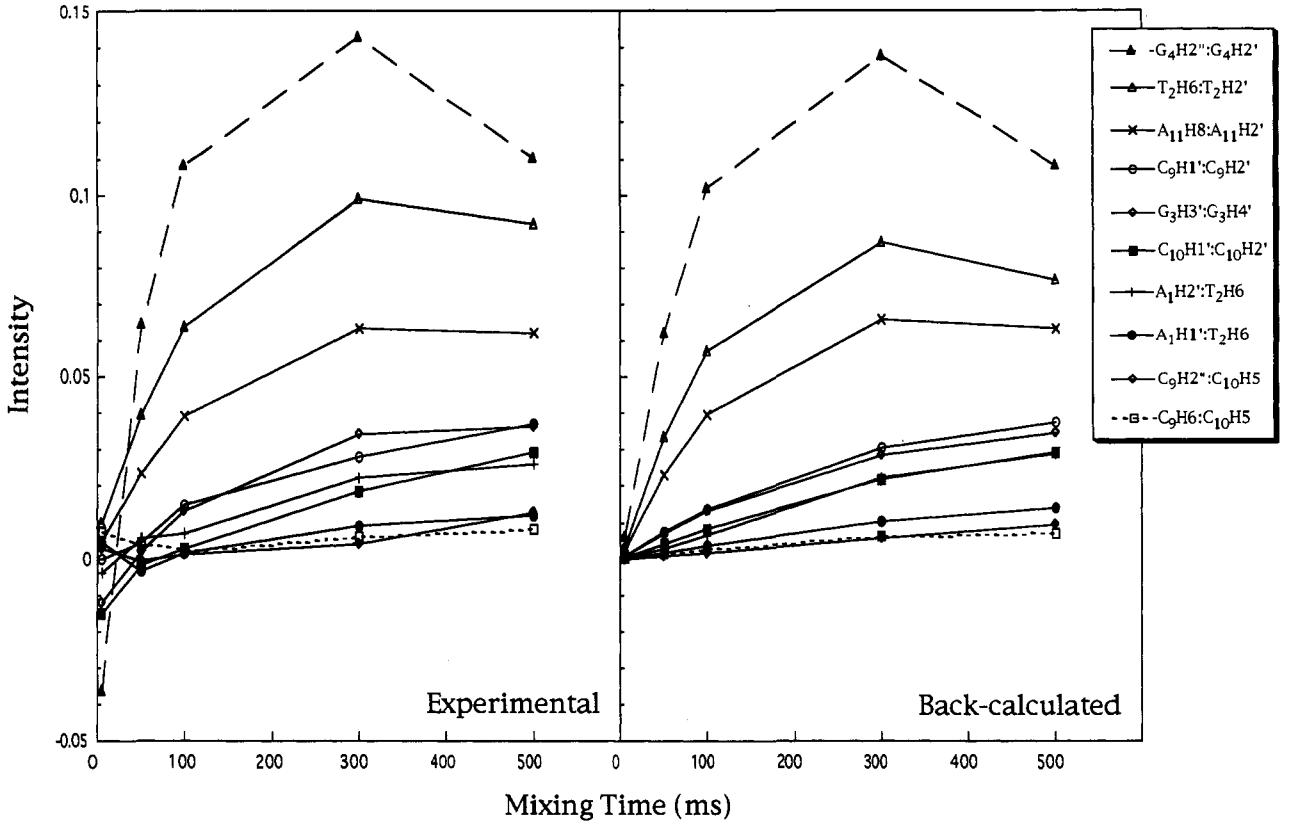

Figure 3. Back-calculated and experimental NOESY buildup curves of the Pt(en)/12-mer.

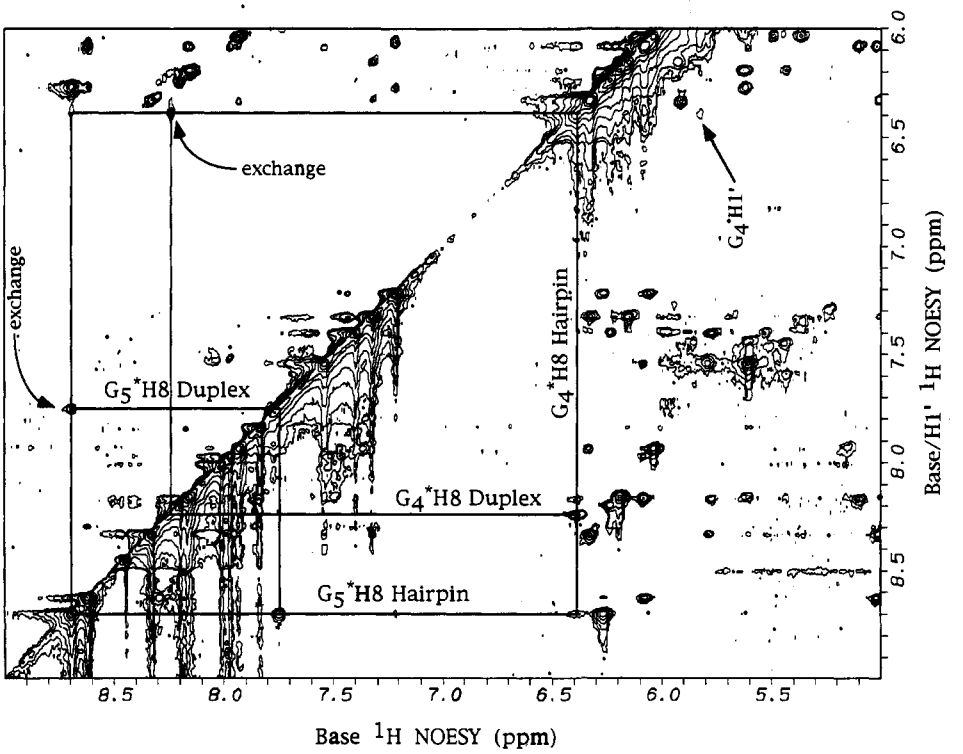

Figure 4. Expanded NOESY spectrum at 30 °C. The region depicted is the base to base and H1'. Noted are the postulated hairpin to duplex exchange peaks for G_5*H8 and G_4*H8.

partner as well. If the G_4*H8 shift of the minor form is in the normal aromatic region, a cross peak between the aromatic and another region should be found in the 30 °C but not in the 5 °C NOESY spectrum. This is indeed the case; a new cross peak was seen between two unidentified signals, one in the aromatic region and one in the H1' region (Figure 4). The signal in the H1' region (6.39 ppm) is the missing G_4*H8. The normal shift of G_4*H8 of the minor form aided in its discovery; however, the relatively small abundance of the minor form makes it very difficult to investigate. Since the minor form has normal G*H8 shifts and is favored by high concentration and low temperature, it is probably a duplex form. Several imino signals associated with

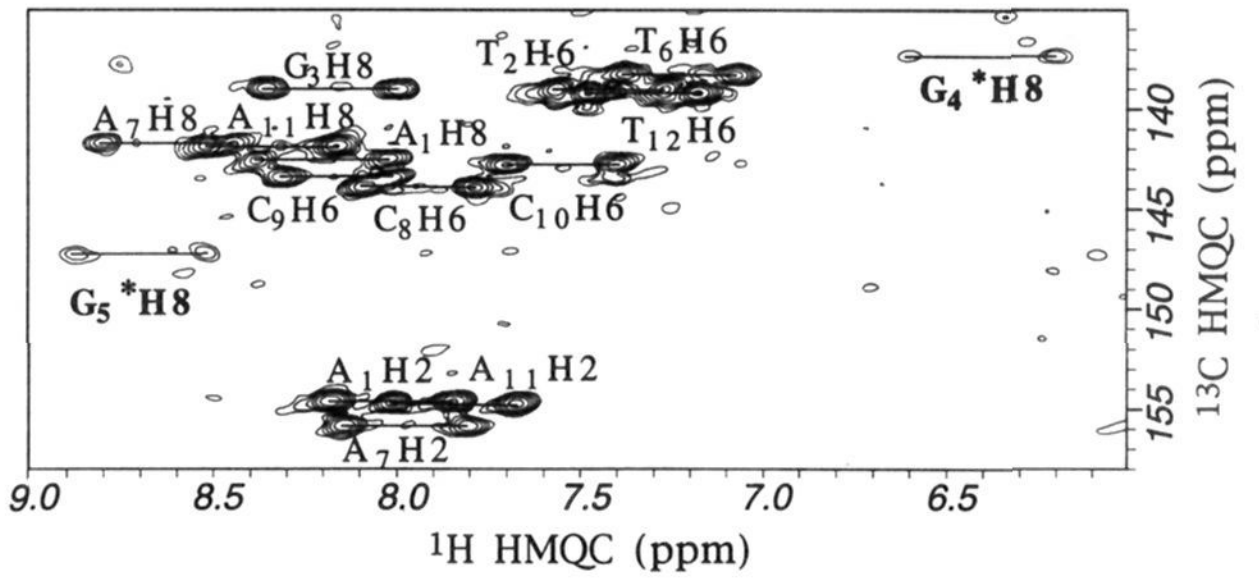

Figure 5. Downfield region of the ^{1}H–^{13}C HMQC spectrum.

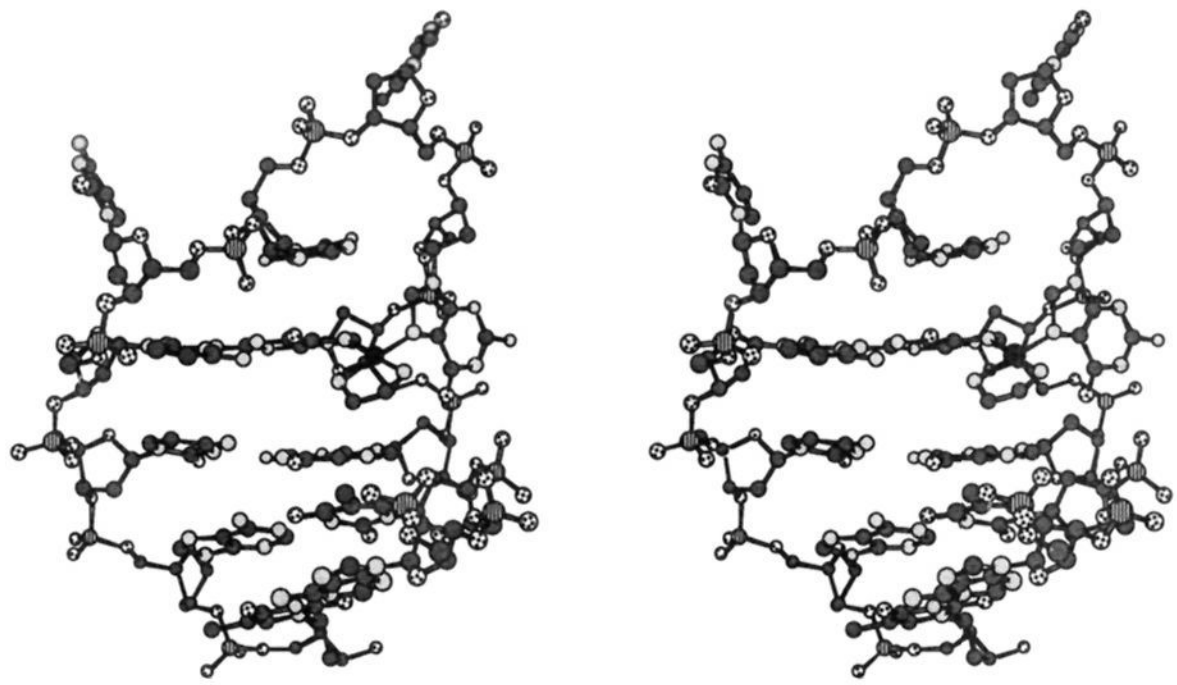

Figure 6. Stereoview of a representative Pt(en)/12-mer structure from a group of 10 low-penalty structures with an RMSD < 0.8 Å for all atoms, including H's.

the minor form in low-temperature H_2O spectra are consistent with a duplex form.

The signal we now assign to G_4*H8 of the major form escaped identification in previous studies because it is broad and overlapped at other temperatures. However, close inspection of NOESY spectra shows that this 6.39 ppm signal has characteristic NOEs to the H1′, H3′, H2′, and H2″ signals assigned independently to the G_4* residue, indicating that it is indeed the G_4*H8 signal. Additionally, the newly found G_4*H8 signal has inter-residue NOEs with the H1′, H3′, H2′, and H2″ signals of G_3.

Examination of the Pt(en/12-mer by ^{1}H–^{13}C HMQC spectroscopy, which has seldom been applied to DNA anticancer drug adducts, has allowed us to confirm the G_4*H8 assignment. In the HMQC spectrum (Figure 5), there is an aromatic ^{13}C signal at 137.4 ppm with a one-bond HMQC cross peak to the broad ^{1}H signal at 6.39 ppm. The aromatic ^{13}C to the H1′ region cross peak confirmed that the 6.39 ppm signal is the elusive G_4*H8.

On platination of G, C8 and H8 signals shift from ~138 and ~7.7 ppm[37] to ~141[23] and 8.3–8.7 ppm,[38] respectively; shift changes on platination (Δ) are normally *downfield* for these signals (~3 ppm for C8 and ~0.6–1 ppm for H8). For the Pt(en)/12-mer (Figure 5), in contrast, both G_4*C8 and G_4*H8 are unexpectedly observed *upfield*, exhibiting wrong-way Δ's. Upfield Δ's have not been observed previously for G*C8 and G*H8; but in 5′G*pG*3′ cross-links, upfield Δ's occur for sugar signals of the 5′G*'s, which have an N sugar pucker.[23] The upfield Δ's[39] of G_4* C3′ (~6.5 ppm), C4′ (~2.5 ppm), and C5′ (~2.5 ppm) indicate that G_4* has an N sugar,[23,24] a feature undetected with ^{1}H NMR data.[1,2] Downfield shift changes of C8, C1′, C3′, and C4′ accompany the *anti* G to *syn* G rotation.[40] The magnitude and direction of the downfield Δ's[39] of G_5* C1′ (~5 ppm), C3′ (~2 ppm), and C4′ (~2.5 ppm) confirm that G_5* has the uncommon *syn* conformation[1,2] with a normal S sugar. Although the ^{13}C shift of a *syn* G*C8 has not been reported previously, one would predict a Δ of ~5–6 ppm from the combined deshielding effects of the *anti* to *syn* rotation (~2–3 ppm)[40] and the heavy-atom effect of Pt (~3 ppm).[23] Thus, the observed Δ for G_5*C8 (147 ppm) of ~9 ppm is unexpectedly large.

^{31}P assignments were determined through the ^{1}H–^{31}P RCSC experiment. These assignments are similar to the ones previously reported[1] with the exception of an interconversion of the G_5*pT_6 (–3.77 ppm) and T_2pG_3 (–3.58 ppm) signals.

DG Structure. The new and previously observed spectral features, many of them unprecedented for any anticancer drug DNA adducts, point to a severely distorted structure induced by the need to balance DNA and Pt structural demands. In order to explain the unusual findings, we conducted distance geometry (DG) calculations, as described above. Broad bounds were generally used in order to sample conformational space sufficiently without too much bias from the NMR data.

In DG models (Figures 6–8 and the supplementary material), the G_4* and G_5* residues are *anti* and *syn*, respectively. The G_5* base is nearly perpendicular to the coordination plane (the usual

(37) Jia, X.; Zon, G.; Marzilli, L. G. *Inorg. Chem.* **1991**, *30*, 228–39.
(38) Kozelka, J.; Fouchet, M.-H.; Chottard, J.-C. *Eur. J. Biochem.* **1992**, *205*, 895–906.
(39) These values are relative to the corrected ^{13}C chemical shifts of the corresponding residue in the unplatinated 12-mer duplex (ref 37).
(40) Wang, Y.; de los Santos, C.; Gao, X.; Greene, K. L.; Live, D. H.; Patel, D. J. *J. Mol. Biol.* **1991**, *222*, 819–32.

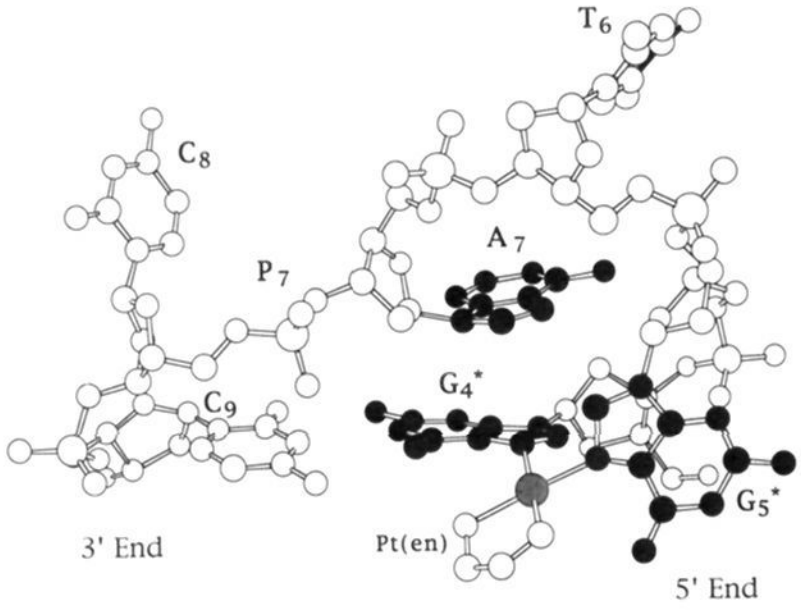

Figure 7. Loop region (G_4* to C_9) of the Pt(en)/12-mer.

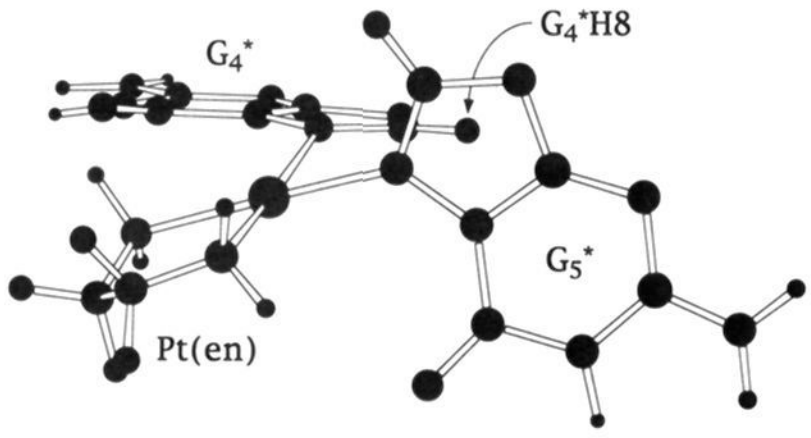

Figure 8. Platination site of the Pt(en)/12-mer.

arrangement), whereas the G_4* base is oriented almost in this plane and is stacked upon G_3. Consequently, the five-membered rings of the G_4* and G_5* bases are forced closer together (Figure 8) than is usual for DNA or cross-linked adducts.[33,41,42] The wrong-way Δ's for G_4* require shielding of $\sim$2 ppm for G_4*H8 and $\sim$3.5 ppm for G_4*C8 to counter the heavy-atom effects. Maximum shielding from a *cis* G* for an *unstrained* structure predicted theoretically is 0.84 ppm.[38,43] Conceivably, in a *strained* structure (G_4*H8–G_5*$\leq$3 Å vs normal $\sim$3.4 Å), the shielding[43] from G_5* could reach 2 ppm for G_4*H8, but not as much as 3.5 ppm for the more distant G_4*C8 ($\sim$3.5 Å). The wrong-way G_4*C8 Δ and the remarkably large downfield G_5*C8 Δ most probably result from different types of strain induced in the bases by the close G_4*–G_5* contact.

The orientation of adjacent coordinated guanines has been the focus of many investigations. Platinated duplex oligonucleotides[4,44,45] normally possess *anti–anti* head-to-head 5′G*pG*3′ cross-links (Scheme 1); however, the Pt(en)/12-mer is best described as having an *anti–syn* head-to-side 5′G*pG*3′ cross-link (defining the head as the C8 end) (Scheme 1). The G_4* base in DG models is not completely coplanar with the platinum coordination plane because of unfavorable van der Waals contacts between the en moiety and G_4*O6. Moreover, the broad G_4*H8 signal suggests a dynamic process that is intermediate on the NMR time scale. Minor vacillation about the Pt–N7 bond could bring G_4*H8 closer to and farther from the anisotropic G_5*. The

Scheme 1. Comparison of the new head-to-side conformation of two *cis* bases to the known head-to-head and head-to-tail conformations.

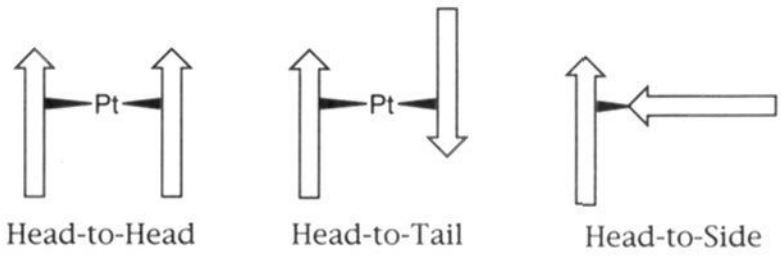

broadness combined with the unusual chemical shift leading to overlap with other signals accounts for the previous failure to locate the G_4*H8 signal.

Distortion of the platination site in the Pt(en)/12-mer structure is additionally reflected in the G_5* γ torsion angle. From COSY data, an *anti* conformation between the G_5*H5′ and the G_5*H4′ protons is evident. The *anti* γ of G_5* places H5′ close to the *syn* base. The downfield shift of H5′ (4.40 ppm) might be the result of the orientation of this proton in the deshielding cone of the *syn* G_5* base.

G_4* has a more common *anti* χ arrangement; however, the sugar of the G_4* residue possesses an N conformation, as indicated by the upfield shifts of G_4* C3′, C4′, and C5′. Solid-state[24] and solution[23] ^{13}C NMR studies have shown that significant upfield shifts of these sugar carbon signals are indicative of the presence of an N sugar conformation. This sugar form has been seen in other platinated oligonucleotides[4,23,44] where typically the 5′-linked G displays the N conformation. A molecular mechanics investigation[46] on platinated oligonucleotide adducts reported that the change in sugar pucker of the 5′-coordinated G from S to N reduces the strain caused by platinum coordination.

In DG models (Figure 7), A_7 is tucked inside the loop on top of G_4*. The proximity of the anisotropic A_7 base to G_4*H2′ ($\sim$3 Å) explains its substantial upfield Δ ($\sim$1.2 ppm[37]) to 1.39 ppm. A_7 base shielding is probably affecting G_4*H8 as well. In addition, A_7H8 is close to G_5*H8 ($\sim$2.3 Å), accounting for the previously reported unusual NOE. The $\sim$0.4 ppm downfield Δ of A_7H8 can be explained in part by A_7H8's location in the deshielding region of G_5*. In the NOESY-in-H_2O spectrum, the A_7 H1′, H2′, and H2″ signals show cross peaks to the G_4*NH1 imino signal. With all of these interactions taken into consideration, the A_7 base seems to be most appropriately located inside the loop above G_4*H8 (imidazole ring) and G_4*H2′ (pyrimidine ring). DG models support this arrangement, and further, the A_7 sugar ring is oriented with C1′ and C2′ pointed toward the G_4* aromatic ring and C3′ away from the loop.

T_6 and C_8 were very difficult to characterize because the T_6 and, less so, C_8 residues are fluxional. Full characterization of fluxional residues via distance geometry is inappropriate.[47] Overlays of structures with T_6 oriented toward the major groove and others with T_6 toward the minor groove are shown in the supplementary material. These structures depict the two extremes of the dynamic motion of T_6. Molecular mechanics/dynamics calculations are needed; however, some general features seem likely.

T_6 displays many NOEs to G_5* as well as to A_7. No single orientation of T_6 in the DG structures accounts for all of these NOEs simultaneously. The large number of NOE cross peaks could result from extensive spin diffusion, but short mixing time data (50–100 ms) suggest that this is not the case. The T_6 base needs to be oriented on the minor groove side to account for cross peaks between T_6Me and G_5*H4′ and on the major groove side to account for cross peaks between T_6Me/H6 and G_5*H2′/H2″.

(41) Admiraal, G.; van der Veer, J. L.; de Graaff, R. A. G.; den Hartog, J. H. J.; Reedijk, J. *J. Am. Chem. Soc.* **1987**, *109*, 592–4.
(42) Schöllhorn, H.; Raudaschl-Sieber, G.; Müller, G.; Thewalt, U.; Lippert, B. *J. Am. Chem. Soc.* **1985**, *107*, 5932–7.
(43) Giessner-Prettre, C.; Pullman, B.; Borer, P. N.; Kan, L.-S.; Ts'o, P. O. P. *Biopolymers* **1976**, *15*, 2277–86.
(44) Herman, F.; Kozelka, J.; Stoven, V.; Guittet, E.; Girault, J.-P.; Huynh-Dinh, T.; Igolen, J.; Lallemand, J.-Y.; Chottard, J.-C. *Eur. J. Biochem.* **1990**, *194*, 119–33.
(45) den Hartog, J. H. J.; Altona, C.; van Boom, J. H.; van der Marel, G. A.; Haasnoot, C. A. G.; Reedijk, J. *J. Biomol. Struct. Dyn.* **1985**, *2*, 1137–55.
(46) Kozelka, J.; Petsko, G. A.; Lippard, S. J. *J. Am. Chem. Soc.* **1985**, *107*, 4079–81.
(47) Patel, D. J.; Shapiro, L. *Annu. Rev. Biophys. Biophys. Chem.* **1987**, *16*, 423–54.

Evidently, the T_6 residue is located primarily outside of the loop in a fast conformational equilibrium between the major and minor grooves.

With regard to residue C_8, the RCSC spectrum shows very strong coupling between C_8H3' and P_8. This coupling gives a strong indication of a *-ac* alignment about the ϵ torsion angle (*i.e.* *syn* arrangement of C_8H3' and P_8, θ). The relatively strong NOEs between C_8H3' and C_9 H5 and H6 and the absence of any inter-residue NOEs with C_8H1' suggest that the C_8 base is outside of the loop (Figure 7) with the C3'/C4' region of the sugar located close to C_9 and the C1'/C2' region more solvent-exposed. Additionally, weak NOESY cross peaks between $C_8H6/H5$ and A_7H4' suggest that the C_8 residue is more toward the H4' side of the A_7 sugar. No cross peaks between the C_8 aromatic signals and A_7H3' or $A_7H2'/H2''$ were present, establishing C_8's location far from this portion of the A_7 sugar. Cu^{2+} line broadening NMR studies[1] have shown that the C_8 base is indeed exposed to solvent. The new NMR data agree well with this conclusion. C_8, being more solvent-exposed, probably exhibits a fair amount of motion.

The DG studies help to explain the pronounced downfield ^{31}P Δ of A_7pC_8 to –2.43 ppm. The downfield ^{31}P Δ is a result of an *anti,anti* conformation of the ζ,α torsion angles[48] induced by the extension of the backbone needed for C_9 to Watson–Crick base pair with G_4* (Figure 7). The G_4*C_9 base pairing is supported by imino proton data. This base pair is at the top of the stem and stacked upon the G_3C_{10} base pair. Evidence for stacking is from NOE data of the exchangeable and nonexchangeable ^1H signals. Cross peaks are seen between G_4*H8 and G_3 H1', H2', and H2'', between C_{10}H6 and C_9 H1', H2', and H2'', and between G_3NH1 and G_4*NH1. Normal stacking of the G_4*C_9 base pair orients G_4*N7, a platinum-binding site, in the major groove. This implies that the platinum drug is in the major groove as well. In low-penalty DG structures, only this conformation was evident. Placement of G_4*N7 and Pt(en) in the major groove requires that G_5*N7, the other platinum-binding site, is in the major groove as well.

The remainder of the stem has a fairly normal B-form structure stabilized by base pairing. This stabilization counters the destabilization induced by the Pt. The resulting structure is a compromise. Both the DNA loop structure and the Pt conformation are unique: neither exists without the other. Thus, we have established parallels between metal DNA adducts and metalloproteins. Metals stabilize specific protein structures, whereas proteins stabilize specific metal geometries such as those optimized for catalytic processes.

Acknowledgment. We thank the National Institutes of Health for financial support (GM 29222).

Supplementary Material Available: Tables of the RMSDs of low-penalty structures in two series, tables of the RMSD penalty values of the same low-penalty structures, tables of penalty violations of sample structures from the two series, and figures of the overlay of low-penalty structures (13 pages). This material is contained in many libraries on microfiche, immediately follows this article in the microfilm version of the journal, and can be ordered from the ACS; see any current masthead page for ordering information.

(48) Gorenstein, D. G. In *Phosphorus-31 NMR. Principles and Applications*; Gorenstein, D. G., Ed.; Academic Press, Inc.: Orlando, FL, 1984; pp 7–36.